Available online at www.sciencedirect.com
SCIENCE DIRECT®
International Journal of Heat and Mass Transfer 48 (2005) 4190–4204
International Journal of HEAT and MASS TRANSFER
www.elsevier.com/locate/ijhmt

# Flow pulsation and baffle's effects on the opposing mixed convection in a vertical channel

Tsai-Shou Chang *, Yann-Huei Shiau

*Department of Power Mechanical Engineering, National Formosa University, 64 Wun-Hua Road, Huwei, Yuenlin 63208, Taiwan ROC*

Received 18 June 2004; received in revised form 31 December 2004

**Abstract**

This numerical study aims to investigate the effects of a horizontal baffle on the heat transfer characteristics of pulsating opposing mixed convection in a parallel vertical open channel. The influences of the dimensionless pulsating frequency Strouhal number and magnitude $A$, Prandtl number and baffle position $L_b$ on the velocity and temperature distribution and long-time average Nusselt number $\langle\overline{Nu}\rangle$ variation for the system at various $Re$ and $Gr/Re^2$ are explored in detail. Our results show that the channel with both flow pulsation and a baffle gives the best heat transfer. With a larger $Re$, the inlet flow pulsation dominates the whole velocity field in the channel. $\langle\overline{Nu}\rangle$ always increases with a larger $Re$, pulsation magnitude $A$ and Prandtl number. Maximum $\langle\overline{Nu}\rangle$ occurs at some specific imposed pulsating frequencies which can be considered to be the natural frequency of the system.


## 1. Introduction

In the past several decades, the capacity of electronic equipments has significantly grown owing to the more compact and quicker IC components contained within a remarkably reduced size. The requirement accompanied with the benefit is to expel the generated heat to the environment in time; otherwise, the IC chip will not function due to overheating. Therefore methods to effectively enhance heat transfer are of interest for many researchers now. Among the heat transfer enhancement schemes, those related to the mixed convection within a vertical channel receive much attention because it often occurs in practice such as in electronic cooling equipments, cooling passages of turbine blades and heat exchangers, etc.

However, in our previous study [1], we found that in a typical situation of opposing mixed convection, the heat transfer is worse if the heat transfer surface is covered by recirculation. It is attributed that heat energy must be first transferred to the recirculating working fluid, then to the cold main stream outside the recirculation by conduction. This conductive heat transfer is owing to that no fluid is exchanged between the main stream and the recirculation. In a later work [2], we utilized a horizontal baffle to alter the direction of the main stream to enhance the heat transfer rate. Again, the results reveal that the flow recirculations beside the heated surface still limit the heat transfer. So, in this article, in additional to installing a horizontal baffle on the channel wall, a periodic inlet velocity oscillation is employed to further increase the heat transfer rate.

A comprehensive review of fundamental flow dynamics and heat transfer of mixed convection can be found in Refs. [3,4].

* Corresponding author.
*E-mail address:* tschang@sunws.nhit.edu.tw (T.-S. Chang).

0017-9310/$ - see front matter © 2005 Elsevier Ltd. All rights reserved.
doi:10.1016/j.ijheatmasstransfer.2004.12.015

**Nomenclature**

| | |
|---|---|
| $b$ | channel spacing |
| $\vec{B}$ | buoyancy force vector |
| $d$ | baffle height |
| $f$ | oscillatory frequency |
| $g$ | gravitational acceleration |
| $Gr$ | Grashof number, $g\beta q_H b^4/kv^2$ |
| $h$ | convective heat transfer coefficient |
| $k$ | thermal conductivity of fluid |
| $\ell$ | length of the heated section |
| $\ell_b$ | $x$-direction distance of the baffle from the heated section |
| $L$ | dimensionless length of the heated section |
| $L_b$ | dimensionless $x$-direction distance of the baffle from the heated section |
| $Nu$ | local Nusselt number |
| $\overline{Nu}$ | space-average Nusselt number |
| $\langle\overline{Nu}\rangle$ | long-time average of $\overline{Nu}$ |
| $p$ | pressure |
| $P$ | dimensionless pressure, $(p-\rho gx)/\rho\bar{u}_e^2$ |
| $Pr$ | Prandtl number, $v/\alpha$ |
| $q_H$ | imposed wall heat flux |
| $Re$ | Reynolds number, $\bar{u}_e b/v$ |
| $St$ | Strouhal number, $f\cdot b/\bar{u}_e$ |
| $T$ | temperature |
| $T_e$ | inlet temperature |
| $u,v$ | dimensional velocities in the $x$ and $y$ direction |
| $u_e$ | inlet velocity |
| $\bar{u}_e$ | average inlet velocity |
| $U,V$ | dimensionless velocities in the $X$ and $Y$ direction |
| $\vec{V}^*$ | provisional velocity vector |
| $x$, $y$ | Cartesian coordinate |
| $X$, $Y$ | dimensionless Cartesian coordinate |

*Greek symbols*

| | |
|---|---|
| $\alpha$ | thermal diffusivity |
| $\beta$ | volumetric thermal expansion coefficient |
| $\delta$ | dimensionless baffle height, $d/b$ |
| $v$ | kinematic viscosity |
| $\theta$ | dimensionless temperature, $\theta=(T-T_e)/(q_H\cdot b/k)$ |
| $\rho$ | density of fluid |
| $\tau$ | dimensionless time |
| $\Delta\tau$ | time increment |

Habchi and Acharya [5] numerically studied the mixed convection of a heated block on a vertical channel to simulate the hot IC component on a vertical PC board. They found that $\overline{Nu}$ would be reduced if a blockage exists. Besides, a recirculation is observed downstream of the blockage with a small temperature difference inside the recirculation. Changing the height of the blockage 0.1–0.2 times of the channel height does not affect the heat transfer rate. Heat transfer of a heated obstacle in a horizontal channel was studied by Young and Vafai [6] via a finite element formulation. The existence of the obstacle results in a significantly changed velocity field and induces recirculations both up- and downstream of the obstacle. Heat transfer rates of upstream and top faces are better than that of the downstream face of the obstacle. Yan et al. [7] used a transient liquid crystal thermograph to investigate the heat transfer enhancement of three in-line, surface-mounted obstacles. Three shapes of obstacles—circular, square, and diamond—are examined. Detailed local heat transfer enhancement was obtained. Besides, through the local heat transfer variation, the flow structure can be reasonably interpreted.

Martinuzzi and Havel [8] experimentally investigated the flow structure between two in-line cubic obstacles. They emphasized the influence of the gap between two obstacles. They found a large recirculation with low turbulence if $S/H<1.4$ where $S$ and $H$ are the distances of the gap and obstacle height, respectively. The separated shear layer produced by the upstream obstacle will impact the downstream obstacle with $1.4<S/H<3.5$. With an $S/H$ larger than 3.5, the wake of the upstream obstacle will reattach in the gap; therefore, a second horseshoe vortex system is found around the downstream obstacle. Valencia and Cid [9] employed the $\kappa$–$\varepsilon$ model to simulate the turbulent hydrodynamic and heat transfer characteristics of two side-by-side square bars in a channel. Herman and Kang [10] adopted the curved vane behind the heated block to alter the flow direction and observed a 1.5–3.5 times enhancement in heat transfer but, in turn, the pressure penalty is 3–5 times larger.

Transitional ($Re=3400$) and fully turbulent ($Re=24\,000$) incoming flow in a periodically ribbed duct was experimentally examined by Acharya et al. [11]. Different heat transfer behaviors were found due to the resulting turbulence levels. Kim and Anand [12] used a two-dimensional $\kappa$–$\varepsilon$ turbulent model and a double cyclic condition to simulate the periodically fully developed flow. They found that the conduction within the substrate plays an important role because of its ability to redistribute the heat transfer and decrease the overall heat resistance. Hwang and Liou [13] discussed the heat transfer and friction in a horizontal channel with perforated ribs on the top and bottom plates. The best thermal performance was found with 44% open-area ratio

perforated ribs. In a later study [14] they examined the effect of thickness of single perforated ribs. Their results reveal that a thinner and taller perforated rib can produce a better heat transfer. Kilicaslan and Sarac [15] experimentally examined the effect of cylindrical and triangular ribs with holographic interferometry. The heat transfer with ribs is much higher than that without ribs. The differences of heat transfer and pressure drop between cylindrical and triangular ribs are negligible. Pressure drop penalty dramatically increased with Reynolds number. Yun and Lee [16] conducted an experiment to investigate several kinds of fin-and-tube heat exchangers with interrupted surfaces in home air conditioners. Webb et al. [17] provided the correlations of Colburn $j$ factor and the fanning friction factor $f$ of seven helically ribbed with several parameters such as rib height, number of start and helix angles.

Greiner et al. [18] used a spectral element technique to explore the heat transfer of a grooved channel. They found that the grooves could enhance the heat transfer but also increase the pressure drop. However, the grooved channel can provide a better heat transfer rate under the same, given pressure drop. Later, in [19], they discuss the effect of flow rate oscillation with a low Reynolds number. The results disclose that a better heat transfer and a lesser pumping power, are obtained when the imposed exciting frequency approaches the natural frequency.

Roughnesses and ribs enhance the heat transfer by breaking the thermal and momentum boundary layers. On the other hand, fins and baffles alter the main flow direction to increase the heat transfer rate. Maughan and Incropera [20,21] numerically and experimentally studied the dependence of heat transfer performance on the periodically longitudinal fins. The results reveal that the gap between the fins dominates the flow pattern and heat transfer. Specially, a worse heat transfer rate was noted with a narrow gap. Dutta and his coworker [22,23] explored the influences of different shapes and arrangements of perforated baffles. Their results indicate that the increase or decrease of heat transfer rate depends on the assigned parameters. Over their investigated ranges, a variation in Reynolds number produces a significant difference. Guo and Anand [24] performed a three-dimensional, numerical simulation to study the effect of installing a baffle near the entry of a horizontal duct. The heat transfer of the upstream surface of the baffle is better than that of the rear surface due to the flow impingement. Wang et al. [25] numerically investigated the heat transfer enhancement resulting from the staggered and/or in-line arrangements of baffles in a periodical, fully developed channel flow. They found a self-sustained unsteady oscillation with a Reynolds number between 100 and 200. This oscillation, in turn, increases the mixing rate between the core flow and the near-wall fluid and, therefore, increases the heat transfer rate. Habib et al. [26] carried out an experimental investigation with $Re$ ranging from 8000 and 18 000. Their results show the flow deflection and impingement upon the fin's response for the heat transfer enhancement.

The characteristics of the pulsating flow and heat transfer in a circular pipe with a porous-medium layer in the pipe surface was numerically studied by Guo et al. [27]. The pulsating flow is driven by the pressure gradient oscillation at the inlet. Brinkman–Forchheimer–extended Darcy mode is adopted for the porous medium. An optimal porous layer thickness is found and related to the ratio of the effective thermal diffusivity. The temperature history inside a porous medium with a periodically oscillating inlet velocity was investigated by Paek et al. [28]. Their results reveal that the temperature history is little affected by the pulsating flow. Hemida et al. [29] found that introduction of a pulsating flow results in a slight decrease of heat transfer in thermally fully developed regions, while in a thermally developing region, heat transfer rate could either increase or decrease depending on the thermal boundary conditions. Camci and Herr [30] employed a communicating loop before a nozzle to produce a self-oscillating impinging planar jet to enhance the forced convection heat transfer. Kim et al. [31] numerically studied the forced convection heat transfer from two heated blocks in a horizontal channel with a uniform and oscillating velocity at the channel inlet. Their results indicate that the natural shedding induced by the upstream block will increase the heat transfer of the downstream block. There is a dominant peak of heat transfer enhancement when the pulsating frequency changes.

Azar [32] utilized a mechanical shaker at the inlet of a vertical channel to enhance the heat transfer of electronic components. Without external forced air, using the shaker will cause a local partial reversal of flow and retard the heat transfer. However, if external forced air is supplied, the temperature of the electronic components will be significantly reduced. Besides, this effect can act both on the upstream and downstream components. Fu et al. [33,34] broke the thermal and momentum boundary layers on a horizontal heated surface by a moving block and a swinging fin to increase the heat transfer.

The above literature review indicates that most of the articles concern about the forced convection in a horizontal channel. However, low speed convection in a vertical channel with a large temperature difference occurring in heat exchangers, cooling of electronic equipments, etc., has not been paid enough attention. This fact motivates the present numerical study. Our objective is to explore the characteristics of heat transfer and hydrodynamics behaviors of the low Reynolds, pulsating mixed convection in a vertical channel with a baffle.

## 2. Analysis

Fig. 1 schematically shows the two-dimensional physical system considered and the coordinates adopted. A vertical parallel channel consists of two infinite plates with spacing $b$. A finite section ($0 \leqslant x \leqslant \ell$) of the left wall is heated by a uniform and constant heat flux $q_H$. The rest of the left wall and the whole right wall are thermally insulated. A downward, forced flow enters the channel at temperature $T_e$ in the far upstream and is assumed to be fully developed. Its magnitude may change sinusoidally with time. An infinitely thin baffle is installed on the right wall. Viscous dissipation is considered to be negligible. Dimensionless governing equations for the unsteady two-dimensional opposing mixed convection for a Boussinesq's flow through a vertical channel with a baffle are:

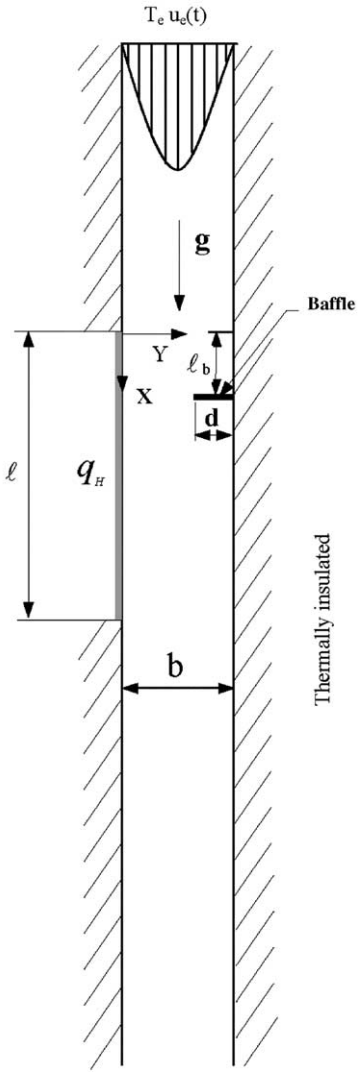


Fig. 1. Schematic diagram of physical system.

Continuity equation:

$$\frac{\partial U}{\partial X}+\frac{\partial V}{\partial Y}=0 \tag{1}$$

$X$-momentum equation:

$$\frac{\partial U}{\partial \tau}+U\frac{\partial U}{\partial X}+V\frac{\partial U}{\partial Y}=-\frac{\partial P}{\partial X}+\frac{1}{Re}\nabla^2 U+\frac{Gr}{Re^2}\theta \tag{2}$$

$Y$-momentum equation:

$$\frac{\partial V}{\partial \tau}+U\frac{\partial V}{\partial X}+V\frac{\partial V}{\partial Y}=-\frac{\partial P}{\partial Y}+\frac{1}{Re}\nabla^2 V \tag{3}$$

Energy equation:

$$\frac{\partial \theta}{\partial \tau}+U\frac{\partial \theta}{\partial X}+V\frac{\partial \theta}{\partial Y}=\frac{1}{Re\cdot Pr}\nabla^2\theta \tag{4}$$

and the associated initial and boundary conditions are

$$\begin{aligned}
&U=6(Y-Y^2), V=0, \theta=0 \quad \text{at } \tau<0\\
&U=6(Y-Y^2)[1+A\,\mathrm{Sin}(2\pi St\tau)], V=0, \theta=0 \quad \text{at } x\to-\infty\\
&\frac{\partial U}{\partial X}=\frac{\partial V}{\partial X}=\frac{\partial \theta}{\partial X}=0 \quad \text{at } x\to\infty\\
&\frac{\partial \theta}{\partial Y}=-1, U=0, V=0 \quad \text{at } Y=0, 0\leqslant X\leqslant L\\
&\frac{\partial \theta}{\partial Y}=0, U=0, V=0 \quad \text{at } Y=0, X<0 \text{ or } X>L\\
&\frac{\partial \theta}{\partial Y}=0, U=V=0 \quad \text{at } Y=1
\end{aligned} \tag{5}$$

The plate spacing $b$ and average inlet velocity $\overline{u_e}$ are used to non-dimensionalize the above governing equations and boundary conditions. The baffle is assumed to be infinitely thin. So, dimensionless temperature and heat flux are both continuous across the baffle. The dimensionless velocities $U$ and $V$ are zero on the baffle surfaces. The local and space-averaged Nusselt numbers of the heated section can be evaluated from the equations

$$Nu=\frac{hb}{k}=\frac{1}{\theta} \quad 0\leqslant X\leqslant L \tag{6}$$

$$\overline{Nu}=\frac{1}{L}\int_0^L Nu\,\mathrm{d}x \tag{7}$$

Since it is possible to have an unsteady $\overline{Nu}$, we also define a time-average Nusselt number

$$\begin{aligned}
\langle\overline{Nu}\rangle &= St\int_{\tau}^{\tau+1/St}\overline{Nu}\,\mathrm{d}\tau \quad \text{for a periodic flow}\\
&= \frac{1}{\tau_2-\tau_1}\int_{\tau_1}^{\tau_2}\overline{Nu}\,\mathrm{d}\tau \quad \text{for a statistical steady flow}
\end{aligned}$$

where $\tau_1$ and $\tau_2$ are two time instants between which is a long enough time interval to have the statistical steady flow.

## 3. Solution method

A well-developed and verified program was modified to numerically solve the time-dependent governing equations and the associated initial and boundary conditions. More details can be found in [1,2]. We briefly describe the numerical method. The projection method [35,36] is employed to numerically integrate the coupled momentum and continuity governing equations, by two steps. First, a provisional velocity vector $\vec{V}^*$ is explicitly computed from previous velocity field $\vec{V}^n$ by ignoring the pressure gradient,

$$\frac{\vec{V}^* - \vec{V}^n}{\Delta\tau} + \vec{V}^n \cdot \nabla\vec{V}^n - \frac{1}{Re}\nabla^2 V^n - \vec{B} = 0 \tag{8}$$

where $\vec{V}^n \cdot \nabla\vec{V}^n$ denotes the convective term, and $\vec{B}$ is the buoyancy force. Then, $\vec{V}^*$ is corrected by including the pressure effect and by enforcing the mass conservation at the next step $n+1$,

$$\frac{\vec{V}^{n+1} - \vec{V}^*}{\Delta\tau} + \nabla P^{n+1} = 0 \tag{9}$$

and

$$\nabla \cdot \vec{V}^{n+1} = 0 \tag{10}$$

Substituting Eq. (9) into Eq. (10) yields the pressure Poisson equation,

$$\nabla^2 P^{n+1} = \frac{1}{\Delta\tau}\nabla\vec{V}^* \tag{11}$$

Once we solved pressure Poisson equation for $P^{n+1}$, we substitute it into Eq. (9) and explicitly calculate $\vec{V}^{n+1}$. The central difference is used to approximate all the derivatives except the convective terms when discretizing the above equations. To enhance numerical stability and accuracy, a third-order upwind scheme [37] is employed to discrete these convective terms. The power-law scheme [38] was used to discrete the energy equation with the time derivative treated implicitly. By using the Conjugated Gradient Squared method [39] to solve the resulting finite-difference equation system, the temperature can be quickly calculated to a very high accuracy. The flow is considered to be steady if the relative error of consecutive iterations is less than $10^{-5}$ for $U$, $V$ and $\theta$ and the overall energy balance is within 0.1%. If the flow cannot reach the steady state, the calculation procedure will continue for a long enough time to obtain a periodic solution or a statistical steady state. Some verifications of the numerical code can be found in [1]. Furthermore numerical verification evidences were given in [2]. We ensure that a $480 \times 48$ gridlines system is suitable in the present work.

## 4. Results and discussion

The foregoing analysis shows that the pulsating, opposing mixed convection in the vertical channel with a baffle is governed by eight dimensionless parameters—the Prandtl number $Pr$, Reynolds number $Re$, ratio of buoyancy to inertia forces $Gr/Re^2$, length of the heated section $L$, inlet velocity pulsating frequency $St$, inlet velocity pulsating magnitude $A$, baffle position $L_b$ and baffle height $\delta$. In order to focus on the effects of baffles and inlet flow pulsation, we assign $L = 20$ and $\delta = 0.5$ in this study. More details about the influences of the two parameters can be found in [2]. In this study, computations were carried out over wide ranges with $Gr/Re^2$ from 0 to $-3.3$, $Re$ from 100 to 500, $St$ from 0.033 to 5, $A$ from 0.05 to 0.8, $L_b$ from 1 to 19.

We first present the results without baffles in order to establish a basic understanding. It is well known that the opposing buoyancy force slows down the flow beside the vertical heated section and reverses the flow direction if the buoyancy force is strong enough. Therefore, the heat transfer is reduced and then increased. The velocity and isotherms of a typical case with $Re = 250$, $Gr/Re^2 = -2.3$, $Pr = 0.71$ at $\tau = 500$ is shown in Fig. 2(a). The ratio of the $X$ and $Y$ axes is set to 1:2 to clearly display the details. The minimum value and increment of the plotted isotherms are both 0.05 in Fig. 2(a) and hereafter. It is illustrated that two recirculations exist beside the heated section, one extends from $X = 0$ to $X = 15$ and the other ranges from $X = 16$ to $X = 25$. If a recirculation exists at any cross-section, for example, at $X = 5$, the velocity $U$ beside the heated section will be less than zero. Therefore, in order to satisfy the mass conservation at that cross-section of the channel, the maximum velocity $U$ of the main stream is greater 1.5. However, this accelerated velocity does not have any advantage to the heat transfer because the major heat transfer mechanism is heat conduction between the recirculation and the main stream.

Between the two recirculations, the main stream attaches to the heated section, and produces a better local heat transfer as can be seen from the denser isotherms around $X = 16$ in the isotherm plot. In addition, through a careful examination of the velocity vector, we found that only a small range upstream of the heated section is affected by buoyancy since the velocity looks like a fully developed velocity profile at $X = -4$.

We next present a series of isotherm and velocity vector plots to illustrate the effect of flow pulsating in Fig. 2(b) with $Pr = 0.71$, $Re = 250$, $Gr/Re^2 = -2.3$, $A = 0.5$ and $St = 0.1$. The sinusoidal inlet velocity is assigned as:

$$U(Y,\tau) = 6Y(1-Y)[1 + A\sin(2\pi St\tau)] \quad \text{at } X \to -\infty$$

where $6Y(1-Y)$ is the $Y$-dependent velocity profile, $A$ the dimensionless pulsating magnitude and $St$ the Strouhal number, dimensionless pulsating frequency. Since

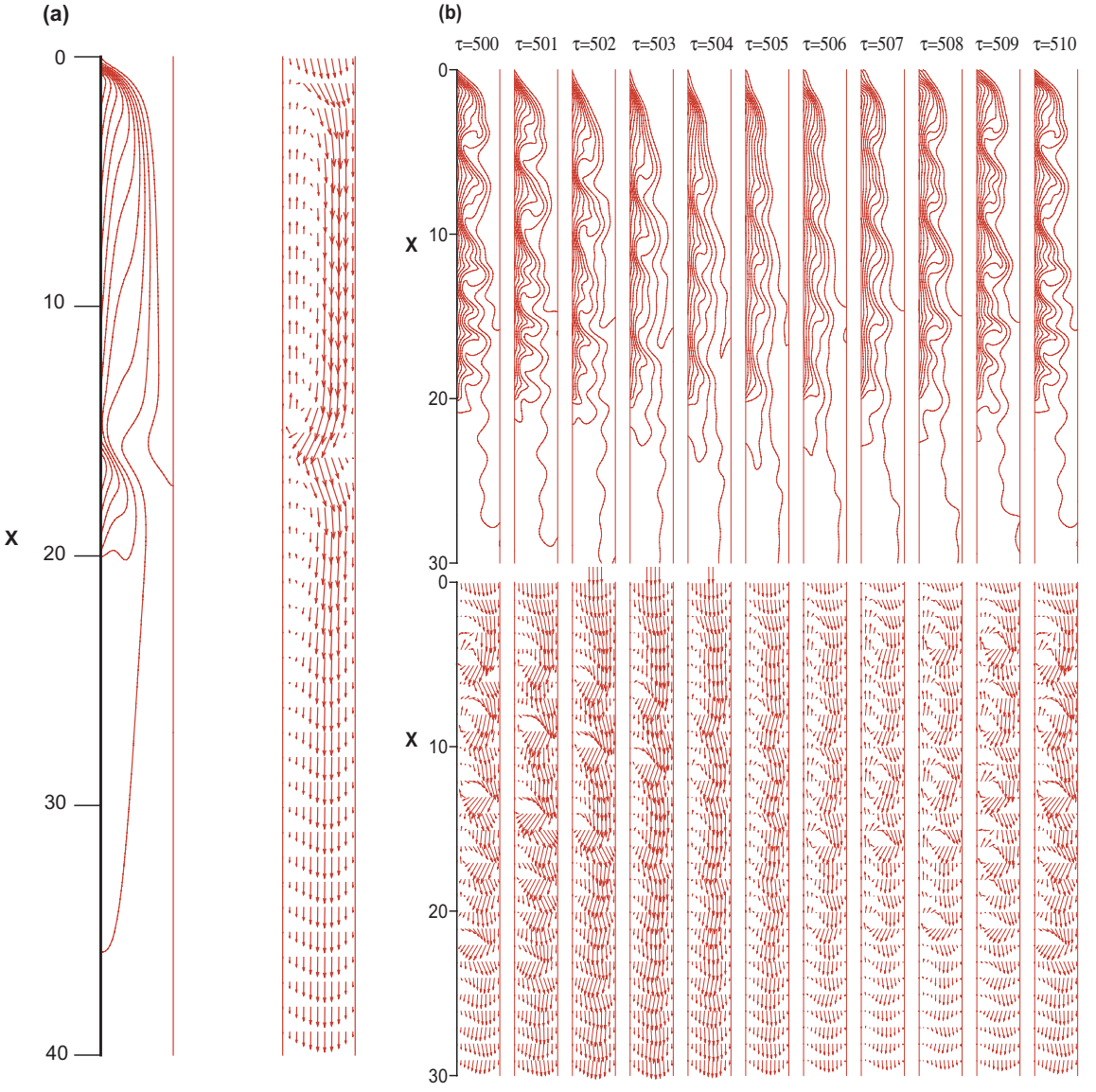


Fig. 2. Isotherms and velocity vector plots of $Re = 250$, $Gr/Re^2 = -2.3$, $Pr = 0.71$. (a) Without baffle and flow pulsation; (b) $A = 0.5$, $St = 0.1$, without baffle; (c) $A = 0.5$, $St = 0.1$ and single baffle at $X = 5$.

$St = 0.1$ implies the time period of the cycle being 10, we draw 11 isotherm plots to show a complete cycle. The time interval between two consecutive plots is one dimensionless time unit. To ensure the plotted cycle being periodic in time, we ran this case for a long enough time and checked the velocity history of the six sampling points. The corresponding dimensionless time instants are labeled above each plot. Considering the oscillating manner of the inlet velocity, we can call the time interval between $\tau = 502.5$ and 507.5 the decelerating phase and the rest of the cycle the accelerating phase [40]. During the decelerating phase, the inlet velocity gradually decreases; therefore, the isotherms around the beginning of the heated section ($X = 0$) gradually move upstream as shown in Fig. 2(b). In the meantime, the isotherms extend transversely. On the other hand, during the accelerating phase, the inlet velocity gradually increases from the minimum to the maximum average inlet velocity and the isotherms are compressed downstream and the heated section. The lower plots are the velocity vector plots at corresponding time instants. We note that more recirculations are generated beside the heated section during the decelerating phase then destroyed during the accelerating phase.

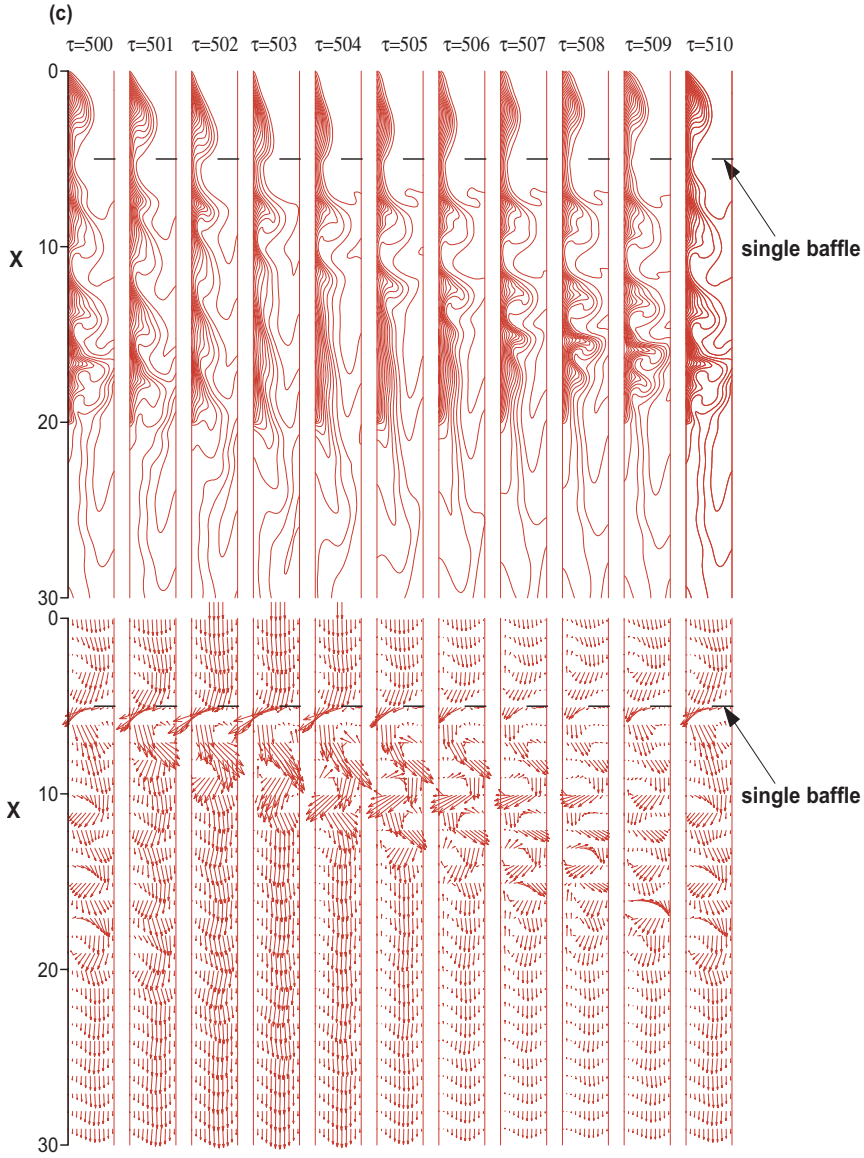


Fig. 2 (*continued*)

Fig. 2(c) demonstrates the effects of installing a horizontal baffle into the vertical channel at $X = 5$ with the same parameters in Fig. 2(b). First of all, the existence of the baffle alters the main stream direction and an obvious concave of isotherms occurs beside the heated section around $X = 5$. During the decelerating phase, the thin thermal boundary at $\tau = 202.5$ gradually becomes thicker and penetrates upward. More recirculations are generated downstream. On the other hand, during the accelerating phase, the thermal boundary layer at the leading edge of the heated section is compressed and the downstream recirculations are swept out. It is worth noting that we observed a time lag between the inlet velocity pulsation and velocity field response during both the accelerating and decelerating phases.

To give more transient behaviors of the fluid, we recorded the local velocity $U$ at six significant locations. These sampling positions are located on the inlet ($X = 0$), middle ($X = 10$) and exit ($X = 20$) of the left ($Y = 0.141$) and right wall ($Y = 0.859$) walls, respectively.

Fig. 3 displays the transient behaviors of velocity $U$ at six sampling points with different $Gr/Re^2$ with $Re = 250$ and $Pr = 0.71$. Fig. 3(a) shows the steady state results with a low opposing buoyancy, $Gr/Re^2 = -0.9$. Beside the heated section, i.e., at $Y = 0.141$, the velocity $U$ is reduced by the opposing buoyancy force. The degree of

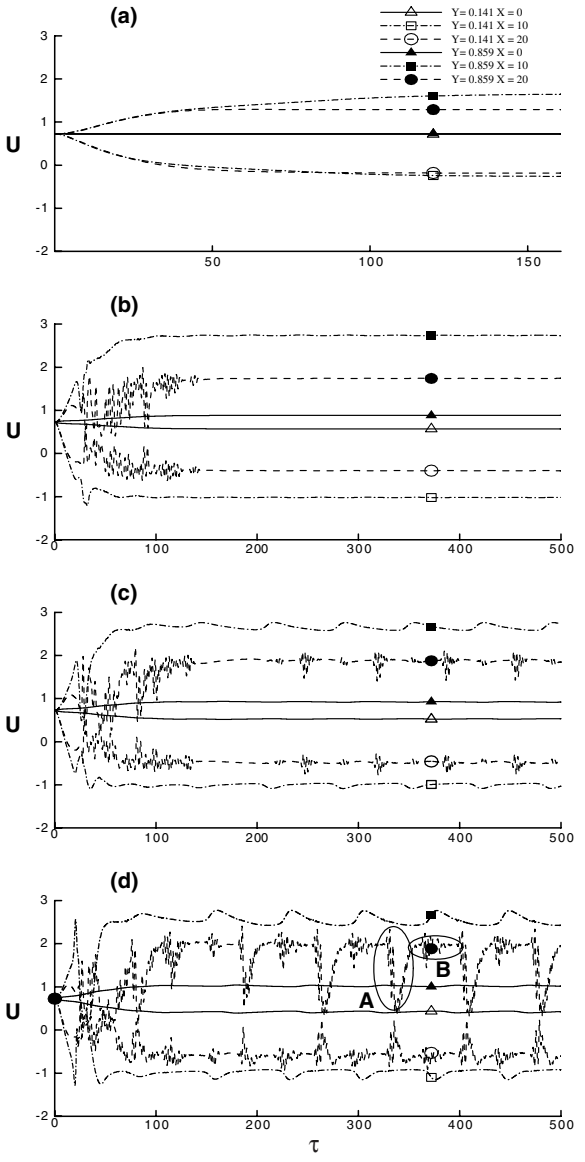


Fig. 3. Velocity $U$ transient behaviors of (a) $Gr/Re^2 = -0.9$, (b) $Gr/Re^2 = -2.3$, (c) $Gr/Re^2 = -2.5$ and (d) $Gr/Re^2 = -2.9$ with $Re = 250$, $Pr = 0.71$ at sampling locations.

velocity reduction increases as the fluid flows downward. On the other hand, the velocities at $Y = 0.859$ are accelerated and are larger than those of the fully developed regime. Another fact which should be noticed is that the negative velocity at $X = 10$ and 20 at steady state implies a recirculation existing over the heated section.

We next increase the opposing buoyancy force to $Gr/Re^2 = -2.3$ while the other parameters remain unchanged and the results are shown in Fig. 3(b). After a violent transient stage, the velocities seem settled down. But, after carefully examining the data, we found that the flow field oscillates slightly and does not approach a steady state. At the starting of the heated section, i.e., $X = 0$, both at $Y = 0.141$ and $Y = 0.859$, the velocities $U$ are still larger than zero, so there is no recirculation. However, at $X = 10$ and $X = 20$, we observe much larger negative velocities and this fact indicates a much strong recirculation.

By further increasing the opposing buoyancy force to $Gr/Re^2 = -2.5$ as shown in Fig. 3(c), the spontaneous oscillation of the velocity is observed at all the sampling locations. At $X = 10$, the oscillating is of a period of about 68.7. A 180° phase lag is found between oscillation history at $Y = 0.141$ and $Y = 0.859$. Much different behaviors occur at $X = 20$, and some ripples or bursts are seen at the transient history. This is an evidence suggesting that the flow becomes transitional around $X = 20$. The ripples have also been observed in temperature transient history, which is not shown here. We explain the mechanism causing the occurrence of ripples as follows. There is a secondary recirculation downstream similar to the one in Fig. 2(a). With a larger opposing buoyancy $Gr/Re^2 = -2.5$, the recirculation occupies more space, consequently, accelerating the main stream. The induced velocity gradient between the main stream and recirculation is great enough to trigger the outside edge of the recirculation to oscillate. Wavelets are periodically generated along the streamlines. When the wavelets travel downstream, they might be amplified or damped out. If they are amplified, some ripples are recorded at $X = 20$. Otherwise, smooth velocity behaviors were found there.

Fig. 3(d) illustrates the transient characteristics with a still greater opposing buoyancy force $Gr/Re^2 = -2.9$. On comparing Fig. 3(c) and (d), we found similar responses at $X = 0$ and 10. However, at $X = 20$, ripples occur all the time. It is worth noting that there exists a sudden deceleration then acceleration process as indicated by ellipse A in Fig. 3(d). Then it followed by a series of bursts in ellipse B. After animating our transient flow field and temperature distribution, the process can be briefly described as follows. At the beginning, the recirculation around $X = 20$ elongates downward to about $X = 26$. It becomes slender and the outside edge suffers from the instability and starts to vibrate horizontally. As the horizontal displacement of the outside edge becomes larger and larger, finally the slender recirculation breaks into two recirculations. The upper recirculation moves backward around $X = 20$. The lower recirculation is convected downstream by the main stream. This elongation then broken process results in the decelerating then accelerating of velocity at $X = 20$.

Next, we will discuss the effects of the periodical inlet velocity on the velocity transient responses of the mixed convection heat transfer. Fig. 4(a) and (b) illustrates the periodic variation of $U$ with dimensionless time at six sampling locations. $Re$, $Pr$, $A$ and $St$ are 250, 0.71, 0.5

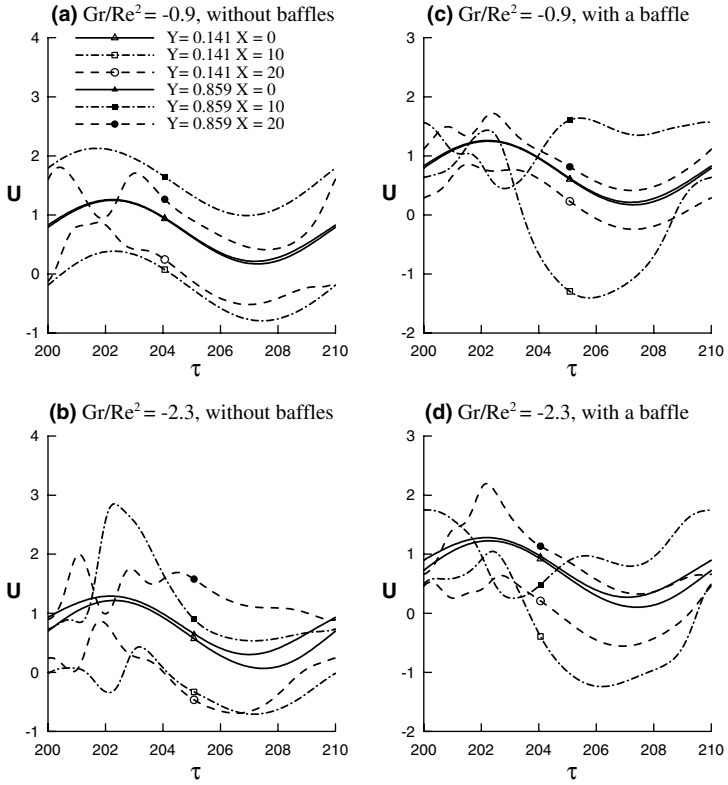


Fig. 4. Effect of $Gr/Re^2$ and baffle on the velocity $U$ transient responses at sampling locations with flow pulsation $A = 0.5$ and $St = 0.1$.

and 0.1, respectively. Since the period of one cycle is reciprocal of $St$, the dimensionless period is 10 in Fig. 4. After a transient variation, all six sampling locations are of the same oscillation frequency equaling the imposed inlet velocity frequency. Therefore only a complete cycle is presented in Fig. 4. However, different behaviors are observed at different locations. In Fig. 4(a), $Gr/Re^2 = -0.9$ at the starting of the heated section ($X = 0$), almost identical velocity histories at $Y = 0.141$ and $Y = 0.859$ are recorded and indicate a symmetrically, longitudinal oscillating at $X = 0$. Similar velocity oscillation with different magnitudes are noted at the middle of the heated section ($X = 10$). The waveforms are of a similar pattern but the magnitudes are different at $Y = 0.141$ and $Y = 0.859$. At the end of the heated section ($X = 20$), out of phase velocities on both the sides appear from $\tau = 200$ to $\tau = 203$. Fig. 4(b) displays the results with a higher opposing buoyancy $Gr/Re^2 = -2.3$. With a high opposing buoyancy force, the velocity–asymmetry range is extended upstream about $X = 10$. Although the oscillation is not sinusoidal but still remains periodic at $X = 10$ and $X = 20$.

Fig. 4(c) and (d) shows the velocity variation on installing a horizontal baffle on the insulated plate at $X = 5$. A comparison of Fig. 4(a) and (c) discloses that a greater oscillation is observed at $X = 10$ in Fig. 4(c). However, at $X = 20$, the oscillation magnitude is smaller

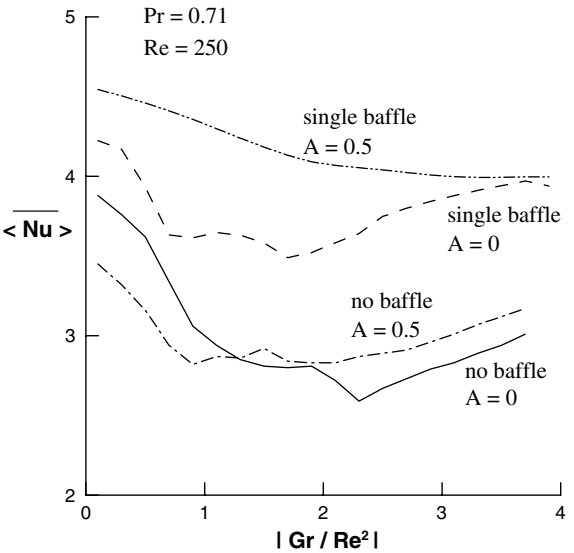


Fig. 5. Effect of various $Gr/Re^2$ on $\langle \overline{Nu} \rangle$ with $Re = 250$, $Pr = 0.71$.

than that in Fig. 4(a) and the time duration with a negative velocity at $Y = 0.141$ is greatly reduced. With a higher opposing buoyancy $Gr/Re^2 = -2.3$, Fig. 4(d) has a similar trend as in Fig. 4(c).

Fig. 5 gives the influence of flow pulsation and a baffle on the long-time average number with various $Gr/Re^2$. Some cases can reach a steady state. For those periodic cases we carried out a time average of the space-average Nusselt number within a complete cycle. For those aperiodic cases, we carried out a long enough calculation to have a statistical-steady average Nusselt number. To provide a basic-line for the parametric analyses and for further comparison, the results without baffles and flow pulsation ($A = 0$) in Fig. 5 is firstly considered. $\langle\overline{Nu}\rangle$ is decreased then increased with the increase of $|Gr/Re^2|$. The increasing opposing buoyancy force reduces the positive velocity beside the heated section and the heat transfer becomes worse. But if the opposing buoyancy force is strong enough, the negative velocity is large enough to recover the heat transfer. The minimum $\langle\overline{Nu}\rangle$ occurs of about $Gr/Re^2 = -2.3$. We next activated the inlet flow pulsation with $A = 0.5$ and $St = 0.1$, but did not install the baffle. A better heat transfer is obtained with $|Gr/Re^2|$ larger than 1.2. In

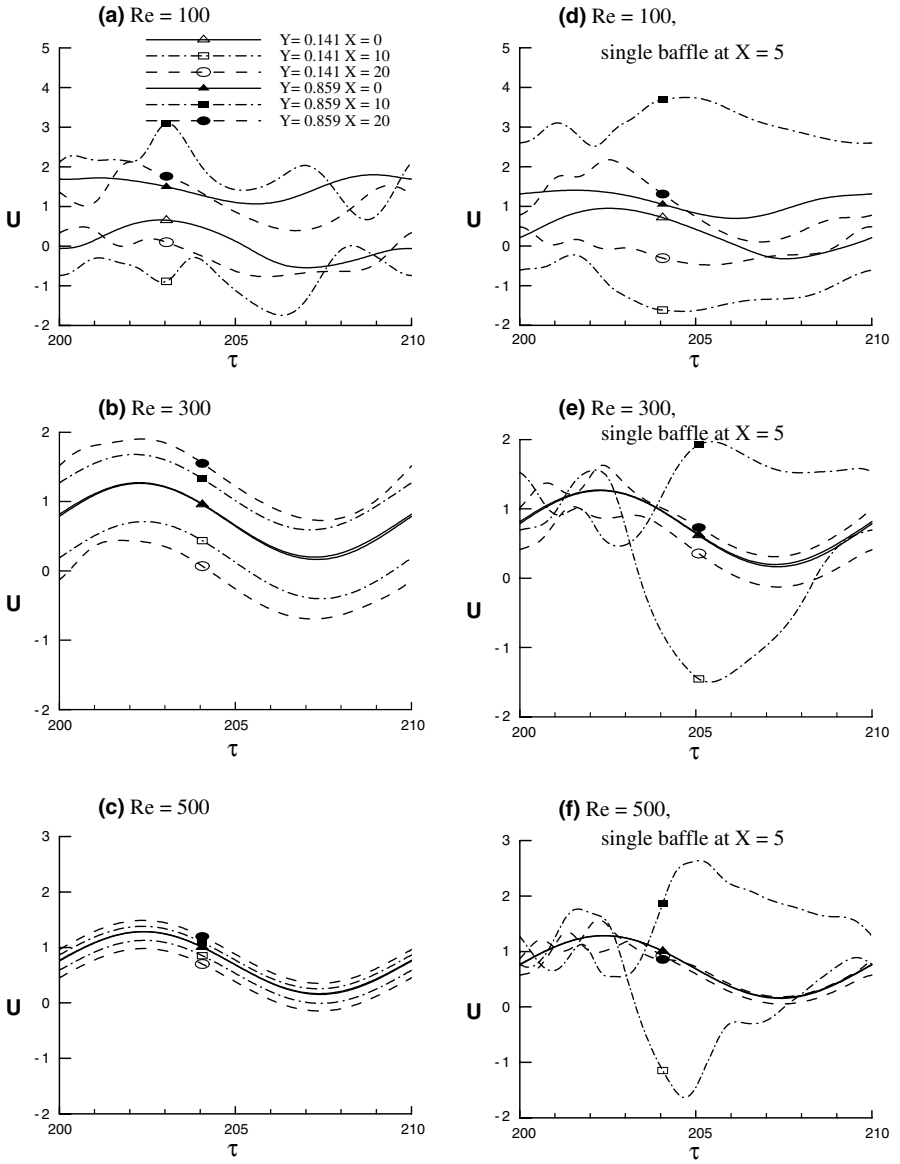


Fig. 6. Effects of $Re$ and baffles on the velocity $U$ transient responses at sampling locations with $Pr = 0.71$, $Gr = 6.25 \times 10^4$, $A = 0.5$ and $St = 0.1$.

contrast, when $|Gr/Re^2| \leqslant 1.2$, $\langle \overline{Nu} \rangle$ without flow pulsation will be larger than that with flow pulsation. Hence, we have an either increased or decreased mixed convection heat transfer depending on the magnitude of $Gr/Re^2$ if the inlet flow pulsation is presented.

A horizontal baffle is installed on the right plate at $X = 5$ and the steady fully developed velocity is imposed at the channel inlet, i.e., without flow pulsation. A much higher $\langle \overline{Nu} \rangle$ is noted over the $|Gr/Re^2|$ range. This contributes to the alteration of the main stream as shown in Fig. 2(c). Generally speaking, $\langle \overline{Nu} \rangle$ first decreases then increases with a minimum occurring at about $Gr/Re^2 = -1.8$.

Finally, when both installing the baffle and imposing flow pulsation, a further higher $\langle \overline{Nu} \rangle$ will be achieved. Additionally over the investigated $|Gr/Re^2|$ range, $\langle \overline{Nu} \rangle$ smoothly and monotonically decreases with an increase in $|Gr/Re^2|$ and there is no $\langle \overline{Nu} \rangle$ minimum. The results shown in Fig. 5 clearly indicates that the optimum heat transfer scheme among the four proposed schemes is the one with both active (flow pulsation) and passive (baffle) methods. Surprisingly, the inlet flow pulsation is not the key point to enhance heat transfer. As clearly shown in Fig. 3(b), the flow pulsation may cause the temperature distribution to vary periodically but the basic heat transfer phenomenon did not change, i.e., most of heated section surface is covered by the recirculations.

Fig. 6 shows the effects of baffles and various Reynolds numbers on the velocity $U$ under the action of the inlet periodic velocity with $Gr = 6.25 \times 10^4$, $Pr = 0.71$, $A = 0.5$ and $St = 0.1$. First, we discuss the results without a baffle and Re varied from 100 to 500 as shown in Fig. 6(a)–(c). Generally speaking, with a fixed $Gr$, a larger Re implies a stronger inertia force, accordingly, the inlet velocity dominates the entire velocity field. In Fig. 6(a), much different velocity behaviors have been observed at six sampling locations due to the complicated interaction between low inertia force ($Re = 100$) and high opposing buoyancy force ($Gr = 6.25 \times 10^4$). On increasing $Re$ to 300 as shown in Fig. 6(b), we note much order oscillations at six locations, although their magnitudes still differ from each other. On further increasing $Re$ to 500 as shown in Fig. 6(c), not only the magnitudes but also the waveform are nearly identical. This fact implies that the inlet velocity controls the whole flow field inside the channel and the influence of the opposing buoyancy force can be neglected.

Fig. 6(d)–(f) is illustrated to depict the effects of installing a horizontal baffle. On comparing Fig. 6(a) and (d), similar velocity variations are noticed at $X = 0$ and $X = 20$, but more regular and sine-like oscillation is found at $X = 10$. As $Re$ is raised to 300, due to a larger velocity and narrower cross-section area, the local velocity around $X = 5$ significantly increases and a dramatic oscillation of the velocity was seen at $X = 10$ in Fig 5(e). Out of phase velocity oscillation is obvious at $X = 10$. A similar phenomenon is found at $X = 20$, too. The results of $Re = 500$ are close to those of $Re = 300$, except for the further larger flow oscillation at $X = 10$ in Fig. 6(f).

The influences of the baffle and flow pulsation on the long-time average Nusselt number with various Reynolds numbers with $Pr = 0.71$, $Gr = 6.25 \times 10^4$ are summarized in Fig. 7. We first discuss the effects of flow pulsation only. As shown in Fig. 7, when $Re$ ranged from 100 to 250, flow pulsation does not produce an apparent difference due to the strong, dominate opposing buoyancy force and the weak inertia force. However, with $Re$ larger than 250, the imposed flow pulsation does reduce the heat transfer, for example, 12% when $Re = 500$. After carefully examining the results, we found that there exists an additional recirculation around $X = 20$ during the decelerating phase and the heat transfer decreases if the flow pulsation is activated ($A = 0.5$).

We next discuss the results with both flow pulsation and a baffle. Obviously, employing both the active (flow pulsation) and passive (installing a horizontal baffle) schemes can dramatically enhance heat transfer. By using a baffle, the cold main flow can be directed toward the heated section to increase the heat transfer. Flow pulsation may change the velocity field around the heated section and the baffle and further increase the heat transfer. We obtain a 42% increase of $\langle \overline{Nu} \rangle$ at $Re = 500$. Also shown in Fig. 7 is a correlation to account for the influence of varied $Re$ on $\langle \overline{Nu} \rangle$ as follows:

$$\langle \overline{Nu} \rangle = 0.0859 Re^{0.7}$$

for $Re$ varying from 100 to 500, with $A = 0.5$, $St = 0.1$, and a single baffle installed at $X = 5$.

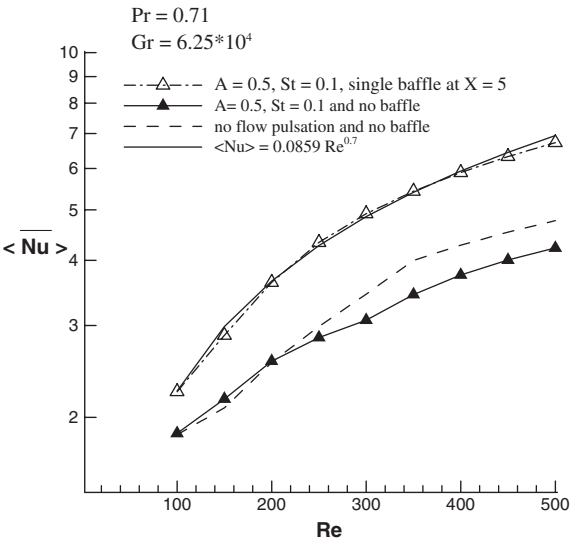


Fig. 7. Influence of varied $Re$ on $\langle \overline{Nu} \rangle$ with $Pr = 0.71$ and $Gr = 6.25 \times 10^4$.

Since the flow pulsation may play an important role in the opposing mixed convection in a vertical channel, we will discuss the effects of pulsating frequency and magnitude.

Fig. 8 illustrates the effects of varying the pulsation magnitude $A$ with $Re = 250$, $Gr/Re^2 = -2$, $Pr = 0.71$ and $St = 0.1$. The results without baffles are shown in Fig. 8(a)–(c). It is obvious that the imposed flow pulsation takes control of the flow field when the magnitude increases from 0.05 to 0.8. Hence, the velocities $U$ at six sampling locations gradually approach to the similar waveform. The same observation is noted in Fig. 8(d)–(f) in which case a horizontal baffle is installed at $X = 5$. More violent flow oscillation is found at $X = 10$ in Fig. 8(e) and (f) because of the baffle and a larger pulsation magnitude.

We now focus on the variation of $\langle \overline{Nu} \rangle$ with pulsation magnitude $A$ as shown in Fig. 9. First of all, we observe that $\langle \overline{Nu} \rangle$ slightly changes with $A$ varied from 0.05 to 0.8 if the baffle does not exist. This is because the flow pulsation may change the flow field and temperature distribution but the long-time, space-average Nusselt number $\langle \overline{Nu} \rangle$ is little affected. In contrast, the existence of a baffle at $X = 5$ can significantly increase the local velocity around the baffle, sweep out the recirculation beside the heated section and enhance the heat transfer.

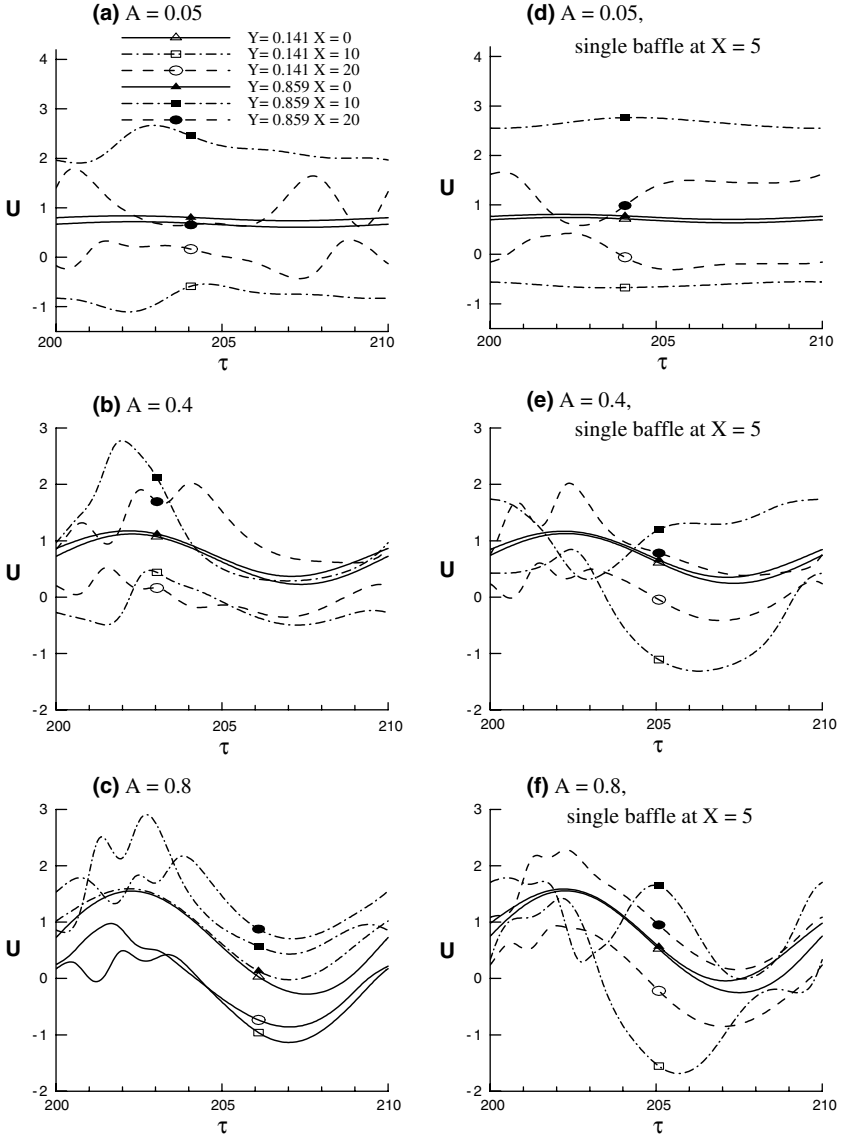


Fig. 8. Effects of pulsating magnitude $A$ and baffles on $\langle \overline{Nu} \rangle$ with $Re = 250$, $Gr/Re^2 = -2$ and $Pr = 0.71$.

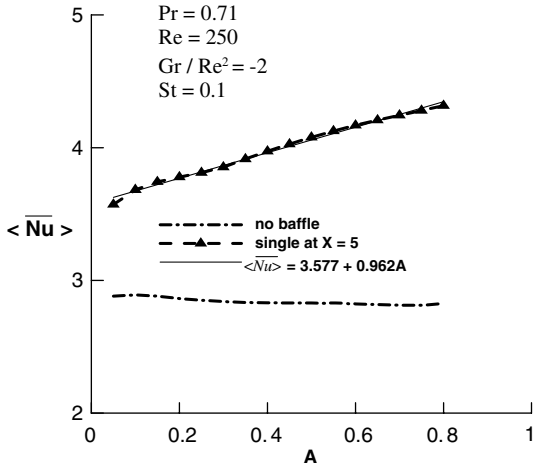


Fig. 9. Influence of $A$ on $\langle \overline{Nu} \rangle$ with $Re = 250$, $Gr/Re^2 = -2$, $St = 0.1$ and $Pr = 0.71$.

Furthermore, this effect becomes more evident with larger magnitudes of $A$. Therefore, the heat transfer enhancement is monotonically increased with $A$. The enhancement is about 23% and 52% for $A = 0.05$ and 0.8, respectively. Based on these numerical results, we propose a correlation of $\langle \overline{Nu} \rangle$ versus $A$:

$$\langle \overline{Nu} \rangle = 3.577 + 0.962A \quad \text{for } A \text{ from } 0.05 \text{ to } 0.8$$

with $Re = 250$, $Pr = 0.71$, $Gr/Re^2 = -2$ and $St = 0.1$.

The variation of $\langle \overline{Nu} \rangle$ with pulsation frequency $St$ is shown in Fig. 10 with $Re = 250$, $Gr/Re^2 = -2$, $Pr = 0.71$ and $A = 0.5$. $\langle \overline{Nu} \rangle$ has local maximuma at $St = 0.25$ and 0.055 for the cases without a baffle. Therefore $St = 0.25$ can be considered to be the natural frequency of this system under the parameter settings. Meanwhile we must point out that a situation with a larger $St$ does not imply a higher heat transfer, at least, over the investigated range. We next discuss the results with a single baffle at $X = 5$. Obviously, better heat transfer is noticed and there are three local maxima with $St = 0.7$, 0.333 and 0.115, respectively. Similarly, an imposed flow pulsation with a too small or too large $St$ will produce a worse heat transfer.

Fig. 11 shows the dependence of long-time average Nusselt number on the Prandtl number with $Re = 250$, $Gr/Re^2 = -2$, $A = 0.5$ and $St = 0.1$. $\langle \overline{Nu} \rangle$ always monotonically increases with $Pr$ and the cases with a baffle at

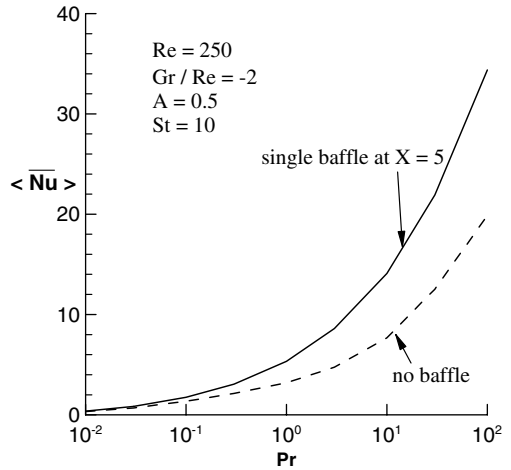


Fig. 11. Dependence of $\langle \overline{Nu} \rangle$ on Prandtl number with $Re = 250$, $Gr/Re^2 = -2$, $A = 0.5$ and $St = 0.1$.

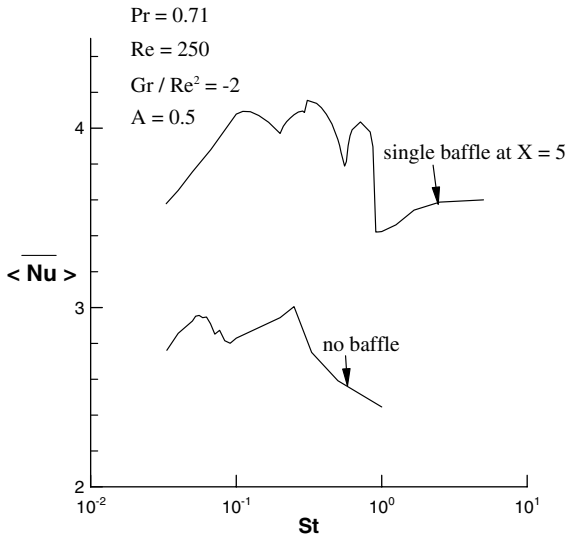


Fig. 10. Dependence of $\langle \overline{Nu} \rangle$ on pulsating frequency $St$ with $Re = 250$, $Gr/Re^2 = -2$, $A = 0.5$ and $Pr = 0.71$.

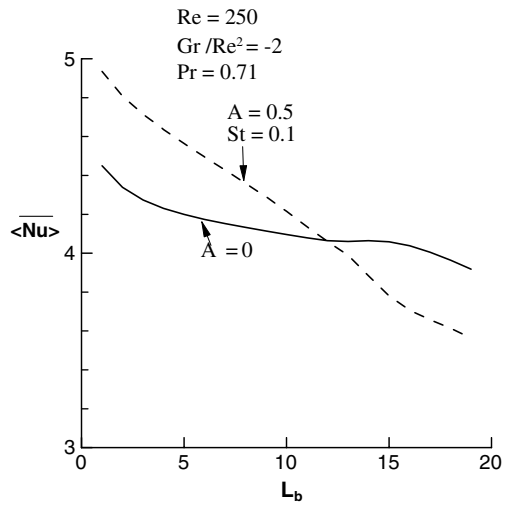


Fig. 12. Dependence of $\langle \overline{Nu} \rangle$ on the baffle position $L_b$ with $Re = 250$, $Gr/Re^2 = -2$ and $Pr = 0.71$.

$X = 5$ have a greater heat transfer. In the meantime, the enhancement of heat transfer also increases with $Pr$. An insignificant difference of $\langle \overline{Nu} \rangle$ is found for the cases with or without a baffle when $Pr = 0.01$. On the other hand, 90% heat transfer enhancement is noted when $Pr = 100$.

Finally, we present the effects of changing the baffle position $L_b$ on $\langle \overline{Nu} \rangle$ with $Re = 250$, $Gr/Re^2 = -2$, and $Pr = 0.71$ in Fig. 12. Generally speaking, a baffle on the upstream will result in a better heat transfer. As the baffle position moves downstream, the heat transfer is reduced. This trend is more evident when the flow pulsation is activated. Additionally, with $L_b < 12$, flow pulsation is useful to increase heat transfer. However, with $L_b > 12$, flow pulsation seems to give a worse heat transfer.

## 5. Conclusions

In this study, a pulsating mixed convection heat transfer in a vertical open channel with a baffle has been numerically investigated. Attention is focused on the effects of the Reynolds number, $Gr/Re^2$, Prandtl number, dimensionless pulsating frequency $St$ and magnitude $A$, and the baffle position $L_b$ on the velocity variation and long-time average Nusselt number. The major results are drawn as follows.

1. The pulsating mixed convection with a baffle gives the greatest heat transfer among the four kinds of combination as shown in Fig. 5 when $Gr/Re^2$ ranges from $-0.1$ to $-3.9$, $Re = 250$, $Pr = 0.71$. A non-pulsating flow with a baffle has a secondary best heat transfer. The stationary or pulsating inlet velocity condition does not affect $\langle \overline{Nu} \rangle$ significantly if a baffle is not installed.
2. The imposed flow pulsation gradually dominates the velocity oscillation in the channel when $Re$ increases. The heat transfer enhancement increases with $Re$.
3. $\langle \overline{Nu} \rangle$ increases with a greater $Re$, pulsation magnitude $A$ and Prandtl number $Pr$. Again, the channel with both flow pulsation and a baffle will generate a better heat transfer.
4. The largest $\langle \overline{Nu} \rangle$ occurs at some certain imposed pulsating frequency, for example, $St = 0.333$ and 0.25 for the channel with and without a baffle installed, respectively. These dimensionless pulsating frequencies can be considered to be the natural frequency of the physical systems.

## Acknowledgements

The financial support of this study by the Engineering Division of National Science Council, ROC, through the contract NSC-91-2212-E-150-037 is greatly appreciated. The authors would like to acknowledge the undergraduate students, Shyh-Chong, Chern and Ming-Hornh, Sheih for carrying out the numerical computations.

## References

[1] T.F. Lin, T.S. Chang, Y.F. Chen, Development of oscillatory asymmetric recirculating flow in transient laminar opposing mixed convection in a symmetrically heated vertical channel, ASME J. Heat Transfer 115 (1993) 342–352.
[2] T.S. Chang, Mixed convective heat transfer in a one-side heated vertical open channel with baffle effect, in: Proceedings of 34th National Heat Transfer Conference, Pittsburgh, Pennsylvania, 2000.
[3] W. Aung, Mixed convection in internal flow, in: S. Kakac, R.K. Shah, W. Aung (Eds.), Handbook of Single-phase Convective Heat Transfer, John Wiley and Sons, New York, 1987 (Chapter 15).
[4] B. Gebhart, Y. Jaluria, R.L. Mahajan, Sammarkia, Buoyancy-induced Flows and Transport, Hemisphere, Washington, DC, 1988 (Chapter 10).
[5] S. Habchi, S. Acharya, Laminar mixed convection in a partially blocked, vertical channel, Int. J. Heat Mass Transfer 29 (1986) 1711–1722.
[6] T.J. Young, K. Vafai, Convective cooling of a heated obstacle in a channel, Int. J. Heat Mass Transfer 41 (1998) 3131–3148.
[7] W.M. Yan, R.C. Hsieh, C.Y. Soong, Experimental study of surface-mounted obstacle effects on heat transfer enhancement by using transient liquid crystal thermograph, ASME J. Heat Transfer 124 (2002) 762–769.
[8] R. Martinuzzi, B. Havel, Turbulent flow around two interfering surface-mounted cubic obstacles in tandem arrangement, ASME J. Heat Transfer 122 (2000) 24–31.
[9] A. Valencia, M. Cid, Turbulent unsteady flow and heat transfer in channels with periodically mounted square bars, Int. J. Heat Mass Transfer 45 (2002) 1661–1673.
[10] C. Herman, E. Kang, Heat transfer enhancement in a grooved channel with curved vanes, Int. J. Heat Mass Transfer 45 (2002) 3741–3757.
[11] S. Acharya, T. Myrum, X. Qiu, S. Sinha, Developing and periodically developed flow, temperature and heat transfer in a ribbed duct, Int. J. Heat Mass Transfer 40 (1997) 461–479.
[12] S.H. Kim, N.K. Anand, Turbulent heat transfer between a series of parallel plates with surface-mounted discrete heat sources, ASME J. Heat Transfer 116 (1994) 577–587.
[13] J.J. Hwang, T.M. Liou, Heat transfer and friction in a low-aspect-ratio rectangular channel with staggered perforated ribs on two opposite walls, ASME J. Heat Transfer 117 (1995) 843–850.
[14] J.J. Hwang, T.Y. Lia, T.M. Liou, Effect of fence thickness on pressure drop and heat transfer in a perforated-fenced channel, Int. J. Heat Mass Transfer 41 (1998) 811–816.
[15] I. Kilicaslan, H.I. Sarac, Enhancement of heat transfer in compact heat exchanger by different type of rib with

holographic interferometry, Exp. Thermal Fluid Sci. 17 (1998) 339–346.
[16] J.Y. Yun, K.S. Lee, Investigation of heat transfer characteristics on various kinds of fin-and-tube heat exchangers with interrupted surfaces, Int. J. Heat Mass Transfer 42 (1999) 2375–2385.
[17] R.L. Webb, R. Narayanamurthy, P. Thors, Heat transfer and friction characteristics of internal helical-rib roughness, ASME J. Heat Transfer 122 (2000) 134–142.
[18] M. Greiner, P.F. Fischer, H.M. Tufo, Two-dimensional simulations of enhanced heat transfer in an intermittently grooved channel, ASME J. Heat Transfer 124 (2002) 538–545.
[19] M. Greiner, P.F. Fischer, H.M. Futo, Numerical simulation of resonant heat transfer augmentation at low Reynolds numbers, ASME J. Heat Transfer 124 (2002) 1109–1175.
[20] J.R. Maughan, F.P. Incropera, Mixed convection heat transfer with longitudinal fins in a horizontal parallel plate channel: Part I—Numerical results, ASME J. Heat Transfer 112 (1990) 612–618.
[21] J.R. Maughan, F.P. Incropera, Mixed convection heat transfer with longitudinal fins in a horizontal parallel plate channel: Part II—Experimental results, ASME J. Heat Transfer 112 (1990) 619–624.
[22] P. Dutta, S. Dutta, Effect of baffle size, perforation, and orientation on internal heat transfer enhancement, Int. J. Heat Mass Transfer 41 (1998) 3005–3013.
[23] S. Dutta, P. Dutta, R.E. Jones, J.A. Khan, Heat transfer coefficient enhancement with perforated baffles, ASME J. Heat Transfer 120 (1998) 795–797.
[24] Z. Guo, N.K. Anand, Three-dimensional heat transfer in a channel with a baffle in the entrance region, Numer. Heat Transfer, Part A 31 (1997) 21–35.
[25] L.B. Wang, F. Ke, S.D. Gao, Y.G. Mei, Local and average characteristics of heat/mass transfer over flat tube bank fin with four vortex generators per tube, ASME J. Heat Transfer 124 (2002) 546–552.
[26] M.A. Habib, A.M. Mobaral, A.M. Attya, A.Z. Aly, Enhanced heat transfer in channels with staggered fins of different spacing, Int. J. Heat Fluid Flow 14 (1993) 185–190.
[27] Z. Guo, S.Y. Kim, H.J. Sung, Pulsating flow and heat transfer in a pipe partially filled with a porous medium, Int. J. Heat Mass Transfer 40 (1997) 4209–4218.
[28] W.J. Paek, B.H. Kang, J.M. Hyun, Transient cool-down of a porous medium in pulsating flow, Int. J. Heat Mass Transfer 42 (1999) 3523–3527.
[29] H.N. Hemida, M.N. SaBry, A. Abdel-Rahim, H. Mansour, Theoretical analysis of heat transfer in laminar pulsating flow, Int. J. Heat Mass Transfer 45 (2002) 1767–1780.
[30] C. Camci, F. Herr, Forced convection heat transfer enhancement using a self-oscillating impinging planar jet, ASME J. Heat Transfer 124 (2002) 770–782.
[31] S.Y. Kim, B.H. Kang, J.M. Hyun, Forced convection heat transfer from two heated blocks in pulsating channel flow, Int. J. Heat Mass Transfer 41 (1998) 625–634.
[32] K. Azar, Enhanced cooling of electric components by flow oscillation, Int. J. Thermophys. Heat Transfer 6 (1992) 700–706.
[33] W.S. Fu, S.J. Yang, A new model for heat transfer of fins swinging back and forth in a flow, Int. J. Heat Mass Transfer 44 (2001) 1687–1697.
[34] W.S. Fu, W.W. Ke, K.N. Wang, Laminar forced convection in a channel with a moving block, Int. J. Heat Mass Transfer 44 (2001) 2385–2394.
[35] A.J. Chorin, Numerical solution of the Navier–Stokes equation, Math. Comput. 22 (1968) 745–762.
[36] R. Temam, On an approximation solution of the Navier–Stokes equation by the method of fraction step: Part 1, Archiv. Ration. Math. Anal. 32 (1968) 135–153.
[37] T. Kawamura, H. Takami, K. Kawahara, New-higher-order up-wind scheme for impressible Navier–Stokes equations, in: Proc. 9th Int. Conf. Num. Math. Fluid Dyn., Springer-Verlag, 1985, pp. 291–295.
[38] S.V. Patankar, Numerical Heat Transfer and Fluid Flow, McGraw-Hill, New York, 1980.
[39] P. Sonneveld, CGS, a fast Lanczos-type solver for non-symmetric linear systems, SIAM J. Sci. Stat. Comput. 10 (1989) 36–52.
[40] T.S. Zhao, P. Cheng, Heat transfer in oscillatory flows, in: C.-L. Tien (Ed.), Annual Review of Heat Transfer IX, 1998 (Chapter 7).